Journal of Experimental Botany, Vol. 71, No. 2 pp. 719–729, 2020
doi:10.1093/jxb/erz200 Advance Access Publication April 30, 2019
This paper is available online free of all access charges (see https://academic.oup.com/jxb/pages/openaccess for further details)

RESEARCH PAPER

The initiation of bud burst in grapevine features dynamic regulation of the apoplastic pore size

Santiago Signorelli[1,2,3,*], Jeremy Shaw[4], Dina Hermawaty[2], Zi Wang[5], Pieter Verboven[5], John A. Considine[2] and Michael J. Considine[1,2,6,7,*]

[1] The School of Molecular Sciences, The University of Western Australia, Perth, WA 6009, Australia
[2] The UWA Institute of Agriculture, and School of Agriculture and Environment, The University of Western Australia, Perth, WA 6009, Australia
[3] Laboratory of Biochemistry, Department of Plant Biology, Universidad de la República, Montevideo, 12900, Uruguay
[4] Centre for Microscopy, Characterisation and Analysis, The University of Western Australia, 35 Stirling Hwy, Crawley, WA, Australia
[5] Division of Mechatronics, Biostatistics and Sensors (MeBioS), KU Leuven, Leuven 3001, Belgium
[6] Department of Primary Industries and Regional Development, South Perth, WA 6151, Australia
[7] Centre for Plant Sciences, School of Biology, University of Leeds, Leeds LS2 9JT, UK

*Correspondence: ssignorelli@fagro.edu.uy or michael.considine@uwa.edu.au

Received 22 November 2017; Editorial decision 12 April 2019; Accepted 16 April 2019

Editor: Robert Hancock, The James Hutton Institute, UK

Abstract

The physiological constraints on bud burst in woody perennials, including vascular development and oxygenation, remain unresolved. Both light and tissue oxygen status have emerged as important cues for vascular development in other systems; however, grapevine buds have only a facultative light requirement, and data on the tissue oxygen status have been confounded by the spatial variability within the bud. Here, we analysed apoplastic development at early stages of grapevine bud burst and combined molecular modelling with histochemical techniques to determine the pore size of cell walls in grapevine buds. The data demonstrate that quiescent grapevine buds were impermeable to apoplastic dyes (acid fuchsin and eosin Y) until after bud burst was established. The molecular exclusion size was calculated to be 2.1 nm, which would exclude most macromolecules except simple sugars and phytohormones until after bud burst. We used micro-computed tomography to demonstrate that tissue oxygen partial pressure data correlated well with structural heterogeneity of the bud and differences in tissue density, confirming that the primary bud complex becomes rapidly and preferentially oxygenated during bud burst. Taken together, our results reveal that the apoplastic porosity is highly regulated during the early stages of bud burst, suggesting a role for vascular development in the initial, rapid oxygenation of the primary bud complex.

Keywords: Apoplast, bud, bud burst, computed tomography, development, dormancy, grapevine, hypoxia, light, oxygen.

Introduction

Grapevine is the most economically important fruit species worldwide, providing fruit for fresh, dried, and processed food and beverage industries, and is grown commercially in >100 countries.The phenology and habit of grapevine are remarkably plastic, displaying strong seasonality and a deciduous habit in temperate regions, while tending towards evergreen in tropical climates (Possingham, 2004).The present understanding of the physiology of these dynamics and the cues that underpin

this plasticity is far from complete (Lavee and May, 1997; Considine and Considine, 2016). Improving this knowledge is important to optimize plant productivity, especially in marginal climates or seasons. In particular, an improved knowledge of the physiology of bud burst is fundamental to enable better canopy management and crop forecasting, as the timing and coordination of this event greatly influence flowering, fruitset, and ripening.

The axillary buds of several species require light for bud burst or outgrowth (Leduc *et al*., 2014). Several grapevine studies have investigated the influence of low-intensity light on bud fruitfulness or shoot physiology, suggesting that it is adapted to a low-light environment (Alleweldt and Hofacker, 1975; May *et al*., 1976; Cartechini and Palliotti, 1995; Petrie and Clingeleffer, 2005; Sánchez and Dokoozlian, 2005). However, there are few reports on the absolute light requirement for bud burst. Although we previously showed that grapevine buds do burst in the absence of light (Meitha *et al*., 2018), there was evidence of light-responsive gene expression well before leaf tips emerge through the scale, indicating perception and early resumption of autotrophic capacities (Signorelli *et al*., 2018). These observations require further physiological elaboration.

Our physiological and molecular data also suggest a developmental role for oxygen (hypoxia) in the initial transition to bud burst (Meitha *et al*., 2015, 2018), corroborating earlier suggestions from gene expression studies (Or *et al*., 2000; Ophir *et al*., 2009; Vergara *et al*., 2012). More than a third of the widely conserved hypoxia-responsive gene homologues and numerous genes with a hypoxia-responsive promoter element were differentially regulated during the first hours of bud burst (Meitha *et al*., 2018). Interestingly, we observed that the internal pO_2 (oxygen partial pressure) minima were peripheral to the meristematic core of the bud following the initiation of bud burst, suggesting an internal source of oxygen (Meitha *et al*., 2015). However, the spatial resolution of the pO_2 data was limited in these studies, which we hypothesize reflects the morphological heterogeneity, within and between biological replicates. If this is the case, coupling this analysis with X-ray micro-computed tomography (μCT) and tissue density and porosity data should reveal direct correlations and provide a more accurate illustration of the spatial variation and magnitude of pO_2 within the bud.

An early indicator of the transition to bud burst is 'sap-flow'; the sudden increase in xylem pressure and the concentration of phytohormones and sugars in xylem sap that precedes bud burst (Skene, 1967; Skene and Antcliff, 1972; Sperry *et al*., 1987). Shoots are known to provide water and nutrients for bud development, until the bud is photosynthetically active and autotrophic (Michailidis *et al*., 2018). A role for callose deposition in gating the symplast during the onset and release of dormancy, metabolically isolating the bud, has been illustrated (Aloni and Peterson, 1991, 1997; Aloni *et al*., 1991; Rinne *et al*., 2011). Yet, further investigation of this role of callose is required (Beauvieux *et al*., 2018), as recent reports showed that callose does not explain the changes in connectivity and the molecular size exclusion limit that occur during development and stress response (Tilsner *et al*., 2016; Nicolas *et al*., 2017). In addition, very little is known of the regulation of apoplastic connections during bud burst, which could play a significant role in delivering long-range signals from the root or shoot to the bud, given the xylem sap pressure and composition. A recent study demonstrated that uptake of the apoplastic dye acid fuchsin is excluded prior to bud burst in grapevine (Xie *et al*., 2018); however, details of how this transition is physiologically regulated deserve further evaluation.

Here we carried out a series of physiological experiments in order to dissect the influences of light, oxygen, and apoplastic connection in the regulation of the initial transition to bud burst. We also defined an apoplastic molecular exclusion size for grapevine buds. These studies also provide important chemical modelling data on two major apoplast-mobile dyes, eosin Y and acid fuchsin. This provides a foundation for further studies of the regulation of vascular connections, and of apoplastic and symplastic transport, between the bud and corpus throughout the annual cycle of perennial buds. It also establishes further confidence in the tissue and developmental dynamics of oxygen content in the bud.

Materials and methods

Plant material and growth under dark and dark–light conditions

Unless otherwise stated, water used throughout the study was Milli-Q® water (MQW, Merck-Millipore, Bayswater, Australia) and chemicals were analytical grade from Sigma-Aldrich (Castle Hill, Australia). Merlot canes containing mature, dormant buds (00 acording to the BBCH scale) from node 3 to 12 were collected from a vineyard in Margaret River, Australia (34°S, 115°E). The canes were transported to the lab and stored at 4 °C until required (no longer than 13 d of storage). Single node cuttings (explants) were prepared as previously described (Meitha *et al*., 2015, 2018), treated by submersion in hydrogen cyanamide (HC) 1.25% (w/v; Sigma #187364) in water for 30 s, and then planted on peat. This was used as an experimental tool to synchronize bud burst in biological replicates, as HC is widely used in industry and experimentally for this purpose. In this respect, we consider that experimental buds were non-dormant. Explants were grown under dark–light (DL, 12 h:12 h) conditions or in complete darkness (D) and used to perform the experiments described below. The photon flux density for the DL condition was between 200 and 300 μmol photons m^{-2} s^{-1}.

Bud burst experiments in D and DL

Trays containing 50 explants each were used to quantify the rate of bud burst in D or DL conditions over 52 d. The experiment was performed four times using samples collected between late April and June (southern hemisphere) in 2016 and 2017; for details refer to Supplementary Table S1 at *JXB* online. The observed response was consistent, with the exception that the time to 50% bud burst decreased as the year progressed, as previously shown in other studies (Or *et al*., 2002; Parada *et al*., 2016). The data presented here represent the explants planted on 5 May 2017. The explants were treated with HC, or untreated, as indicated in the Results. The trays containing the explants were irrigated with potable tap water every second day to ensure a field capacity (FC) of at least 80%. All the trays were filled with substrate to the same weight, and control trays were used to determine the dry weight and the weight at 100% FC. From these data, we determine how much water we should add to reach 80% FC.

CO_2 release and O_2 consumption

CO_2 production was measured as described previously (Meitha *et al*., 2015, 2018). In brief, at least four pools (n=4) of eight excised buds each were placed on a thin layer of sticky tape to avoid dehydration through the base of the bud and were placed in an insect respiration chamber

(6400-89; Li-COR, Lincoln, NE, USA) covered by aluminium foil, which was attached to a Li-6400XT portable gas exchange system to determine CO_2 levels. The measurements were performed in complete darkness, at 23 °C, in CO_2-controlled air (380 µmol CO_2 mol^{-1} air) with 100 µmol m^{-2} s^{-1} air flow, at 55–75% relative humidity.

Oxygen consumption was determined with five pools (n=5) of eight buds each. The buds were placed in a 4 ml micro-respiration chamber (Unisense, Aarhus, Denmark) and the pO_2 was monitored for at least 10 min using an O_2 microsensor (Clark-type, Unisense). The calibration of the sensor was performed by determining the potential at 0% pO_2 and atmospheric pO_2. Calibration of the 0% O_2 condition was achieved by flushing N_2 into the calibration chamber until reaching a constant reading, whereas the atmospheric pO_2 was determined by flushing air into the chamber and taking into account the temperature of the room. Measurements were performed at 23 °C in complete darkness and keeping the micro-respiration chamber under water to prevent sudden changes in temperature. As a negative control, every day the pO_2 in an empty micro-respiration chamber was also measured five times for 10 min each. The average of the slopes obtained with an empty chamber was subtracted from the measurements of the samples. The volume of the buds was determined using a 25 ml density bottle. This information was necessary to determine for each replicate the final volume of air in the chamber.

Following measurement of the CO_2 release and O_2 consumption, the buds were dried in an oven for 72 h at 70 °C to determine the DW, and the respiration rates were calculated. Note that respiratory quotient (RQ) values cannot be calculated from these data because the conditions of measurements are different for CO_2 and O_2. The experiment was repeated three times (Supplementary Table S1).

Apoplastic connection

Both acid fuchsin and eosinY solutions were prepared by dissolving 0.5 g of the respective dye in 0.01 M phosphate buffer pH 6.0. The solutions were filtered through a 9 cm Whatman® GF/A glass fibre filter (W&R Balston Limited, UK) and then through a 0.2 µm membrane filter (Filtropur S 0.2, Sarstedt, Cat. No. 83.1826.001, Nümbrecht, Germany). Explants were sampled from growth conditions at the corresponding times, cut 1.5 cm beneath the bud, and immediately transferred to 25 ml plastic tubes containing 2 ml of eosin Y or acid fuchsin solutions. Unless otherwise stated, the incubation time in the solution was 24 h. A razor blade was used to make a longitudinal cut through the centre of the buds, and the images were taken using a Nikon D700 digital camera (Nikon Inc., Tokyo, Japan) attached to a STEMI SV 8 stereo microscope (Zeiss, Oberkochen, Germany). At least four replicates were used per dye per time (n=4). The experiment was repeated twice (Supplementary Table S1) and both are presented here (Supplementary Figs S1, S2).

Molecular modelling

The geometrical structure of associated and dissociated forms of rhodamine green, acid fuchsin, and eosin Y was fully optimized in aqueous solution at the B3LYP/6-31G(d,p) level integrated with the IEF-PCM polarizable continuum model without imposing symmetry restrictions and using solute cavities adapted to the molecular shape and constructed with Bondi radii. The nature of each minimum was verified by inspection of the eigenvalues of the analytic Hessian in aqueous solution. Optimizations were performed at 298.15 K in the Gaussian09 program. All the calculations were performed using Gaussian09, rev. A.1 (Frisch *et al.*, 2009). To visualize the molecules, animate the vibrational modes, and represent the electron density and the charges, the program Gaussview 9.0 was used. The solvent-accessible surfaces (or Lee–Richards surfaces) were determined using Jmol (Jmol Team, 2007).

Bud porosity and humidity

Five sets of five buds each (n=5) were used to determine moisture content and porosity. Each bud was dissected to separate the scale, trichomes, and green tissues. The porosity and moisture were measured for each tissue. Fresh weight was recorded before measuring porosity. After measuring the porosity, the tissues were desiccated during 96 h in an oven at 70 °C and the dry weight determined. The moisture content was determined as follows:

$$\text{Moisture } (\%) = 100 \times (\text{FW} - \text{DW})/\text{FW}$$

To determine the porosity, the volume of the tissues and the volume of air in the tissues were determined using a density bottle (Thomson *et al.*, 1990). The porosity was measured as follows:

$$\text{Porosity } (\%) = 100 \times \text{Volume of gas in the tissue}/\text{Volume of tissue}$$

Vascular connection and porosity by micro-computed tomography

Grapevine canes collected on 10 May 2016 were sent to Belgium via World Courier and kept at a constant 4 °C. The explants (BBCH scale: 00) were planted on 23 May 2016 in D and DL as was done for bud burst analysis. Three buds of each condition (0, 48, 72, and 168 h each of D and DL) were incubated overnight with caesium iodide (CsI) 10% at 4 °C. 3D imaging using µCT was performed on each bud (BBCH scale: 00-01). µCT was performed with a nanofocus CT system (Phoenix Nanotom, General Electric, Heidelberg, Germany) before and after incubation. For scanning, buds were mounted on the rotation stage by means of a Parafilm wrap. A total of 2400 projection images per scan were taken with 0.15 ° angular steps for a full 360 ° rotation. Capture time for each image was 500 ms. Settings were 55 kV/182 µA for control samples, and 60 kV/167 µA for CsI samples. Image pixel resolution was 2.50–3.25 µm, depending on bud dimensions. Slice reconstruction was performed by Octopus Reconstruction version 8.9.0.9 (XRE, Ghent, Belgium) using the filtered back-projection method.

3D image rendering and quantitative image processing was conducted in Avizo 9.6 (ThermoFisher Scientific, Bordeaux, France). First, the bud volume was masked from the background and the Parafilm wrap used for scanning. This was achieved by applying a global threshold on the grey scale images complemented with erosion, dilation, and filling operations on orthogonal image slices and the 3D volume. Secondly, the pixels inside each masked bud image were assigned to air or bud tissue using a simple grey scale threshold. Pixel values ≤60 (on a 0–255 scale) were assigned to air, according to the grey scale range of the background. Pixel values >60 were assigned to the tissue. Finally, different subsamples (with a representative volume >100×100×100 pixels) of the different parts of the bud (outer and inner scales, trichomes, and base) were taken from the 3D image to calculate local porosity. Porosity was defined as the proportion of total volume of air to the total volume of the subsample. Porosity values of tissues were averages of three buds per condition.

Internal pO_2 profiles

The internal O_2 (pO_2) was measured using an O_2 microsensor (Clark-type, Unisense) with a 25 µm tip as previously described (Meitha *et al.*, 2015, 2018). The calibration of the sensor and measurements were done using the Sensortrace Suite software. For calibration of 0 kPa O_2, the sensor was flushed with N_2 until stabilization, and for normal pO_2 concentration, a fish pump was used to flush the sensor with atmospheric air. The buds were removed from the cane and stood on a flat surface, and then the electrode was electronically inserted from the top to reach the centre of the meristem as described in Meitha *et al.* (2015). The depth of the path changed depending on the size of the bud, but it was usually between 2900 µm and 3700 µm with steps of 36 µm and three measurements per step. The profiles were performed in at least eight buds for each condition and time (n=8). The experiment was repeated three times (Supplementary Table S1) and the last one is presented here.

Electrode pathway by micro-computed tomography

The buds used to determine the internal pO_2 were preserved in FPA solution [10% (v/v) 37% formalin; 5% (v/v) propionic acid; 50% (v/v) 70%

ethanol; 35% (v/v) deionized water] at 4 °C. The samples were subsequently incubated overnight in 1% iodine+2% potassium iodide solution (IKI) in phosphate-buffered saline (PBS) prior to μCT scanning. Buds were then placed in a 5 mm diameter sealed plastic straw in PBS and scanned at 40 kV and 66 μA using a μCT system (Versa 520 XRM, Zeiss) running Scout and Scan software (v10.6.2005.12038, Zeiss). A total of 2501 projections were collected over 360°, each with a 5 s exposure; 2× binning was used to achieve a suitable signal to noise ratio and 0.4× optical magnification was used to achieve an isotropic voxel resolution of 7.9 μm. An LE1 source filter was also applied. Raw data were reconstructed using XMReconstructor software (v10.7.3679.13921, Zeiss) following a standard centre shift and beam hardening correction. The standard 0.7 kernel size recon filter setting was also used. Avizo (v8.1.1, FEI) software was used to obtain orthogonal slices through the data in the same plane as the electrode pathway. Images were then taken into Adobe Photoshop Elements 15 where the pO_2 profiles were mapped onto the electrode pathway. Pixel density was determined using the Line probe tool of Avizo 8.1, as a measure of tissue density. In particular, two lines were used, one just above the path and the other just below the path. The average of the intensities was used to estimate the density of tissue that the probe penetrated.

Statistical analysis

ANOVA was performed for the respiration rate (n=4–5), porosity and moisture by weight (n=5), and porosity by μCT (n=3) experiments, and means from the results from experiments were compared using Tukey's test at the P-values specified in each figure.

Results

The role of vascular development during bud burst and the effect of light

The influence of light on the rate of bud burst was evaluated in the presence or absence of HC, a commonly used agent to synchronize bud burst. The data demonstrated an interaction between light and HC, whereby the influence of light was greater in the absence of HC (Supplementary Fig. S1A, B). HC alone had a considerable effect of increasing the rate of bud burst, accelerating the rate to achieve 50% bud burst from ~28 d to 15 d (in light). For subsequent experiments, we chose to work with HC-treated buds because bud emergence was more predictable than in untreated buds. Bud respiration was also determined in the presence and absence of light (DL and D, respectively) during the first week of growth (0, 48, 96, and 168 h). In both light conditions at 168 h, the CO_2 release and O_2 consumption were greater than at 0 h (Supplementary Fig. S1C, D).

In these conditions, we investigated the vascular development of the buds visually and by μCT to address whether light influenced the resumption of vascular transport. From the μCT data, vascular development was apparent over the time course; however, the contrast agent (caesium iodide) was transported even at 0 h, demonstrating that the vascular tissue was sufficiently functional to transport water and minerals (Fig. 1A and Supplementary Movie S1 show the uptake of the contrast agent in a 3D bud structure). We also investigated whether the apoplast is regulated during the resumption of bud growth in our experimental conditions, using apoplastic dyes which are larger than the contrast agent used for μCT and more reflective of macromolecules transported in the phloem and xylem. Here, dye movement was not evident until after the swollen stage (168 h, 7 d), when bud break was advanced (Fig. 1B, C). The ability of the apoplast to transport the dyes was observed earlier in the DL condition, despite the fact that D-grown buds had reached a similar degree of bud swell over the same time (Supplementary Figs S2, S3). In addition, we observed that the uptake of acid fuchsin was more rapid and extensive than that of eosin Y.

Since the transpiration rate in a later stage of bud burst should be faster than in an earlier stage, it is plausible that the greater uptake of dyes at later stages is due to the greater transpiration, rather than a change in apoplastic connectivity. Thus, we performed an experiment comparing bursting buds with 0 h buds that had been peeled in order to increase the dehydration of the bud, and therefore the uptake of the solution. Our results demonstrate that in an intact bursting explant (216 h), the dye penetrated to the top of the bud within 3 h of incubation (Supplementary Fig. S4A). Nevertheless, in a 0 h peeled bud, even after 72 h of incubation, the dye could not penetrate the buds (Supplementary Fig. S4A). This demonstrates that the observations of Fig. 1B and C are methodologically supported, and that prior to bud burst, bulk flow driven by the xylem pressure or diffusion would still be restricted.

Determination of the molecular exclusion size in buds

To estimate the molecular exclusion size in grapevine buds, the molecules of acid fuchsin and eosin Y, together with rhodamine green as a positive control, were computationally modelled in the associated (neutral) and dissociated forms. The molecular volume, determined by the electron density of the optimized structures, was greater for eosin Y than for the other molecules (Fig. 2A). Indeed, the molecular volume (Supplementary Fig. S5) positively correlated with the molecular weight of the molecules, being the lowest for rhodamine green (Supplementary Fig. S5). The charges and the electrostatic potential of these molecules were also evaluated to understand if their different mobilities are due to different physical–chemical properties. In the associated form, the charges and dipole moment of rhodamine green and eosin Y are quite similar, with the partial charges homogenously distributed through the molecules (Fig. 2B). In the case of neutral acid fuchsin, more extreme partial charges were localized towards the phosphate groups; however, the dipole moment was also small due to the symmetry of the molecule (Fig. 2A). Similar observations were found in the dissociated forms, with regards to the fact that the anionic form of eosin Y had a much greater dipole moment (Fig. 2A). In addition, more extreme electrostatic potentials were found in rhodamine green and acid fuchsin than in eosin Y (Fig. 2C).

To better estimate the required size to transport the molecules through the plant, the solvent-accessible surface for both molecules in the ionic form was modelled (Fig. 3), and the lowest area that they required to be transported was estimated. Our results demonstrated that eosin Y requires a bigger pore area to pass through (Fig. 3). Considering that these soluble molecules will require at least one layer of water hydration shell (~3.5 Å; Laage *et al.*, 2017), the diameter of the pore should be increased by 0.7 nm. Hence, the 1.5 nm estimated length of

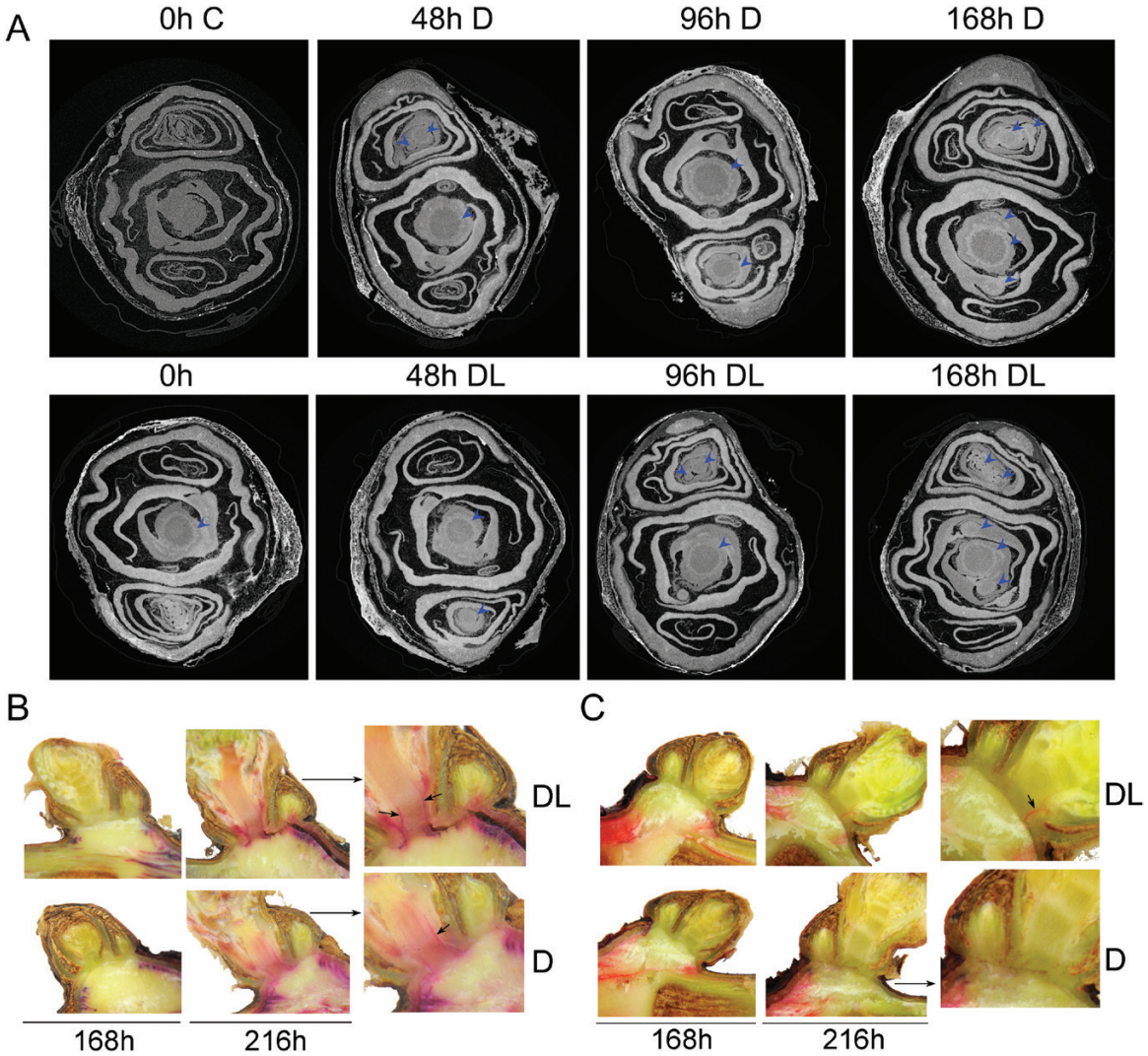

Fig. 1. Effect of light on vascular development. Micro-computed tomography of buds (A). 0 h C refers to 0 h buds untreated with the contrast agent caesium iodide (CsI). All the other buds were treated with contrast agent in order to visualize the vascular tissue (observed as rings and indicated with blue arrows); Apoplastic connectivity evidenced by acid fuchsin (B) and eosin Y (C) staining. Arrows in the magnified image indicate eosin Y staining. Refer also to Supplementary data files.

these molecules would be increased to ~2.2 nm when having one water layer. As we demonstrated that these dyes cannot enter the bud prior to bud burst, but considering that rhodamine green can, we conclude that the molecular exclusion size at the base of the bud is ~2.1 nm.

Determining the tissue-specific oxygen levels in a perennial bud

To investigate further the roles of light and O_2 on the course and coordination of bud burst, we assessed the internal tissue oxygen status (pO_2) through bud burst in the DL and D buds. A slight decrease in the pO_2 over the first 48 h and a marginal increase after 48 h was observed (Supplementray Fig. S6). We then investigated whether light (in assay conditions) can affect the pO_2 in 168 h buds, which were more likely to have developed a photosynthetic capacity. The presence of light during measurement did not significantly increase the internal pO_2 profile in buds grown in the presence (DL) or absence (D) of light (Supplementary Fig. S7A), although we observed a small increase in pO_2 in the peripheral region of the bud (depth 0–200 μm) in the DL condition (>15 kPa, compared with D at <10 kPa; Supplementary Fig. S7B).

The spatial variance among the pO_2 data was considerable (Supplementary Fig. S6), which we hypthosized was due to the considerable tissue heterogeneity within and between biological replicates, confounding the resolution of treatment effects. In order to explore this, μCT was performed on individual buds after assaying the internal pO_2 profile (168 h D and DL). In μCT, the electrode path was clearly visible, enabling us to overlap the pO_2 profile with the images (Fig. 4). As the profile supported our hypothesis, a line probe, reporting the intensity of the pixels, was used to estimate the density of tissue just above and below the electrode pathway. The pO_2 profile correlated well with the internal structure of the bud, as the sudden decline in pO_2 correlated with the probe entering into bract structures, while the pO_2 of the regions of the trichome hairs was elevated (Fig. 4). This analysis also clearly illustrated

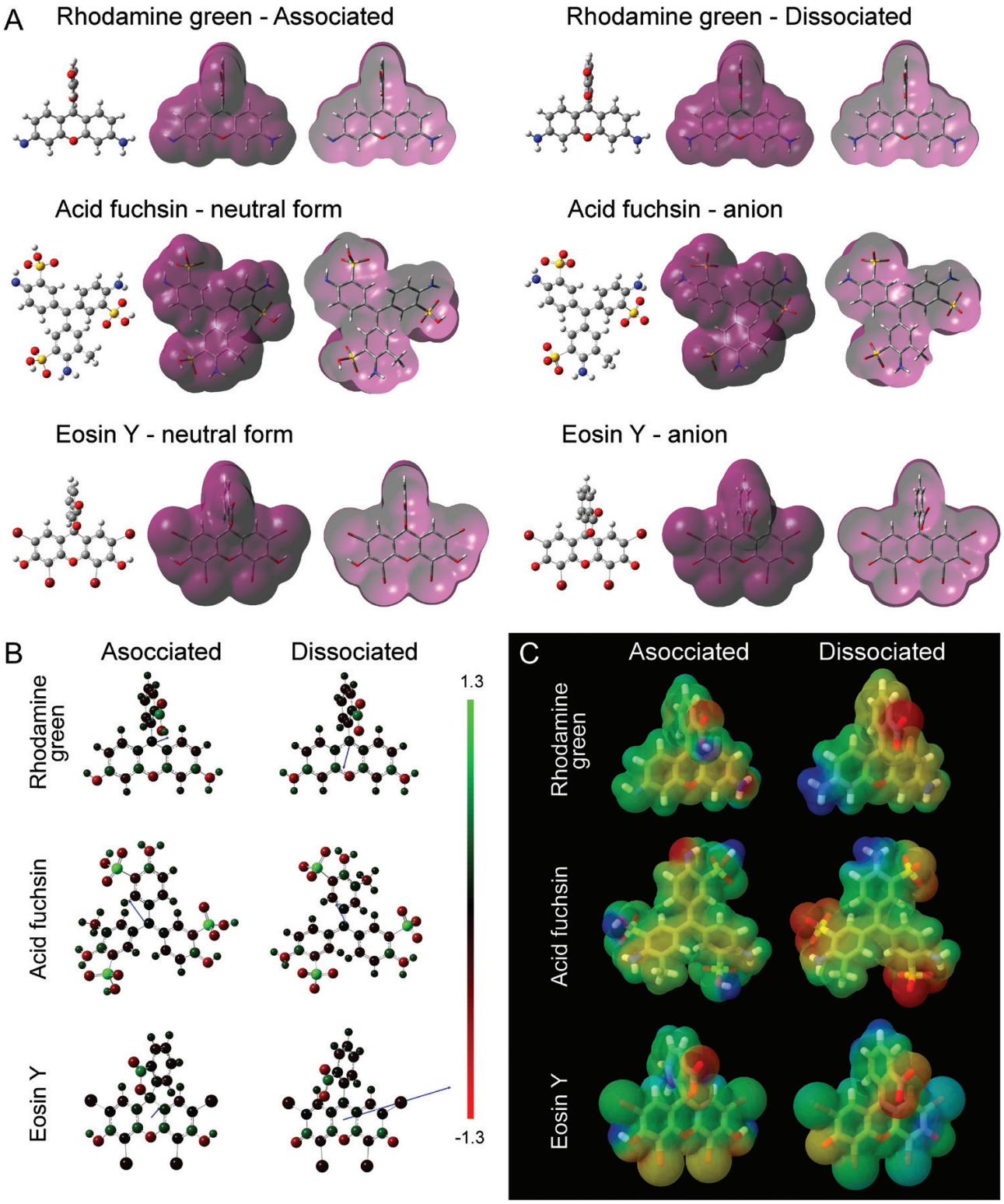

Fig. 2. Chemical modelling of rhodamine green, acid fuchsin, and eosin Y in their associated and dissociated forms. (A) Optimized structure and electron density. Electron density was generated using an isovalue of 0.0004. (B) Charges and dipole moments. The colours indicate the charge and the blue arrows indicate the dipole moment. (C) Electrostatic potentials. Red indicates electronegative zones, whereas blue indicates electropositive zones.

that the pO_2 of the meristematic core of the bud (between 2000 μm and 2400 μm depth) was elevated following the initiation of bud burst.

Exploring the structural context further, we then determined the tissue porosity and moisture content, two variables known to affect O_2 diffusion, of the scales, the trichomes, and the green tissue of grapevine buds (Fig. 5A). These variables were first determined by weight and volume data. The greatest porosity (% gas spaces per unit tissue volume) was found in the trichomes, 77%, followed by 30% for the outer scales and 12%

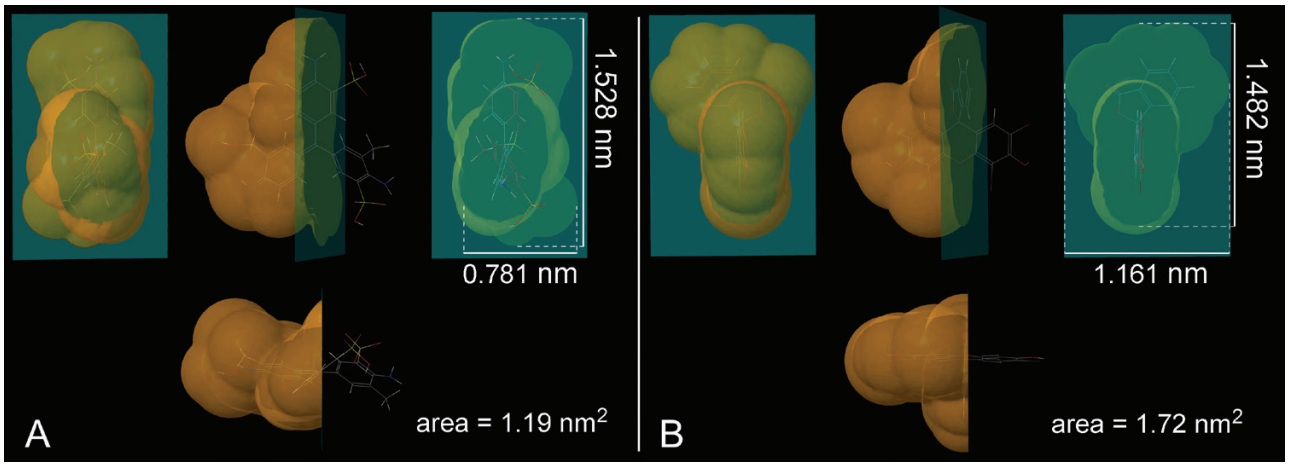

Fig. 3. Solvent-accessible surfaces for ionic forms of acid fuchsin and eosin Y. Anionic acid fuchsin (A) and anionic eosin Y (B). A lateral, frontal, and top view of each molecule is reported, together with the rough area of a pore that they need to pass through.

for the green tissue. Humidity (% water per unit tissue weight) was the lowest for the trichomes (14%), 18% for the scales, and 41% for the green tissue. We further investigated the porosity analysing the structural data obtained by μCT, being able also to evaluate the porosity of the base of the bud, the trichome, bracts, and outer scales (Fig. 5B). The values were 85–88% for the trichomes, 37–38% for the outer scale, 5–6% for the bracts, and 8–10% for the base, at 0 h and 168 h (Fig. 5C). Overall, the results of porosity from the structural images correlated well with the other results. However, the differences between the tissues were enhanced. No statistically significant differences were observed between 0 h and 168 h in terms of porosity of the tissues.

Discussion

An increasing number of studies have added to the literature on signalling and transcriptional changes in bud quiescence, dormancy, and outgrowth/burst. Here we have returned to more classical physiological experiments to establish an improved platform of knowledge to which the gene expression and signalling studies can be related, including non-cell-autonomous signals such as proteins, mRNAs, and miRNAs, and the role of molecular oxygen.

The apoplast pore size of quiescent grapevine buds restricts passive transport to water and small molecules

In the weeks prior to bud burst in woody perennials, xylem pressure builds to extreme levels and becomes enriched in phytohormones and simple sugars (Skene and Antcliff, 1972; Sperry *et al.*, 1987). It has been shown that the symplast is gated during this transition, in a manner dependent on temperature- and gibberellic acid- (GA) regulated glucanases (Rinne *et al.*, 2011). However, given the extreme pressure in the xylem, the apoplast could be a considerable pathway for long-range signals from the corpus (mother vine/tree), which triggers bud burst. Recently, xylem differentiation of grapevine bud was shown to commence in spring at the swelling stage of bud burst (BBCH >5) (Xie *et al.*, 2018). Here we have shown that the aperture of the apoplast between the bud and the corpus is rapidly regulated during the initiation of bud burst, irrespective of the time of the year at which samples were harvested. The data also suggest that the difference in the rates of bud burst observed between D- and DL-grown buds results, in part, from more rapid apoplastic development in the DL condition (Supplementary Fig. S1A).

The isolation of the bud from the corpus during dormancy has long been considered. However, there were no data reporting quantifiable measures of this isolation, such as the molecular exclusion size of buds. The apoplastic transport is limited by the pores formed in the cellulose/hemicellulose fibre structure. Depending on the tissue, the limiting diameter of these pores can vary. In grapevine buds, considering that rhodamine green was shown to be transported (Jones *et al.*, 2000), the information of acid fuchsin and eosin Y was used to determine the pore size of the apoplast in grapevine prior to bud burst (Supplementary Fig. S5). Our value of 2.1 nm diameter pore size in buds is much lower than those observed in other tissues. For instance, in hair cells of *Raphanus sativus* roots and fibres of *Gossypium hirsutum*, the pore size was as small as 3.5–3.8 nm, while in the parenchyma cells of the leaves of *Xanthium strumarium* and *Commelina communis* they were determined to be between 4.5 nm and 5.2 nm (Carpita *et al.*, 1979). In citrus leaves, the size exclusion limit to move through the cell wall and into the phloem was estimated to be between 4.5 nm and 5.4 nm (Etxeberria *et al.*, 2016). The smaller value observed here in grapevine buds suggests that quiescent buds are quite well isolated. However, mono- and disaccharides, such as glucose and sucrose, and phytohormones, such as ethylene, salicylic acid, abscisic acid, jasmonic acid, and GA, should be able to pass though this small pore. Considerable evidence shows that the xylem pressure builds and the sap becomes enriched with simple sugars and phytohormones, particularly cytokinins, in the weeks prior to bud burst (Skene and Antcliff, 1972; Sperry *et al.*, 1987; Maurel *et al.*, 2004; Bonhomme *et al.*, 2010). Our data indicate that these smaller molecules would be capable of being delivered to the meristematic cells of the

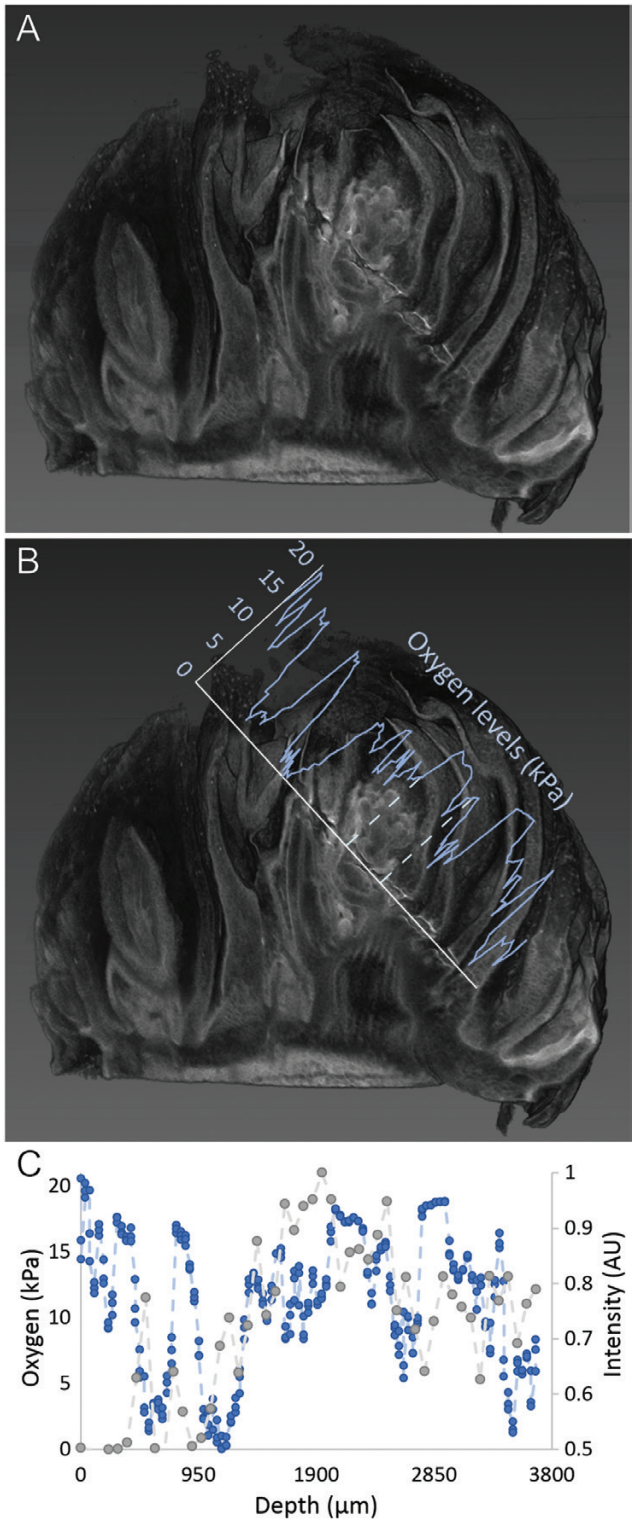

Fig. 4. Internal oxygen profiles and micro-computed tomography of a grapevine bud. (A) 3D structure of the bud showing the electrode path. (B) O_2 profile graph overlapped with the path of the electrode. (C) Internal O_2 profile overlapped with the intensity of the signal determined by a probe line over the path in the µCT. This figure represents the analysis of one bud (corresponding to DL at 168 h). A total of 12 buds used for internal O_2 were scanned by µCT including 0 h, 168 h D, and 168 h DL.

bud via the apoplast, but not larger oligosaccharides, peptides, or macromolecules which may have signalling roles. Cell wall invertase (CWI) may play a key role in mediating the transport of sugars through the apoplast, since sucrose mobility will be more limited than for hexoses. CWI has demonstrated functions in sink strength and regulating developmental transitions and shoot architecture (Heyer *et al.*, 2004). In fact, CWI activity was induced shortly before bud break in buds of peach trees (Maurel *et al.*, 2004), and gene expression of a vacuolar invertase was rapidly induced at the onset of bud burst in grapevine, together with sucrose synthases (Meitha *et al.*, 2018). Bonhomme *et al.* (2010) showed that by early spring, the sugars were transported from the bark and xylem to the bud, at least 1 month prior to bud burst. This suggests that the *de novo* transport of sugars from the cane is not the trigger of bud burst. Rather, the increase in temperature within the bud is important to enable catabolism and secondary active transport of sugars within the bud, resulting in an increase in sink strength, which triggers a commitment to bud burst.

The fact that the pore size of the apoplastic connection is smaller in buds than in roots and leaves of other plants suggests that the isolation of the bud is key to enable desiccation and metabolic quiescence, and to avoid premature rehydration of the bud, which may result in precocious bud burst. A relevant comparison can be made to the seed coat (testa), which is known to protect the plant embryo and can restrict the transport of molecules as small as 2.8±1.2 nm (Kurepa *et al.*, 2010). When the seeds are imbibed, the mucilage of the epidermal cells is hydrated, rupturing the cell wall (Kurepa *et al.*, 2010). Similarly, we observed that morphological changes to bring about an increase in the pore size and allow the transport of these dyes must occur during the early stages of bud burst. Our evidence suggests that pore size increases to >2.1 nm over the course of bud burst to allow the diffusion of eosin Y. Importantly, here we have used computational chemistry to model the structure of the dyes at the quantum level, rather than a broadly estimated size of the molecule, as commonly used in studies reporting transport of nanomolecules. This information itself is highly valuable given that these dyes are widely employed across the life sciences to evaluate vascular transport. The use of a similar approach with symplastic dyes during bud burst would also be very helpful, in light of the evidence of regulation during dormancy transitions.

Light accelerates the reactivation of vascular tissue between the cane and the bud

Light is an absolute requirement for bud burst (outgrowth) in many species, including *Rosa* spp. and pea (Leduc *et al.*, 2014). Here we have shown that grapevine buds have a facultative requirement for light, which accelerates vascular development and the rate of bud burst, but not the final proportion of buds burst. This effect was not due to a more developed state of the buds grown in DL conditions; in fact, less developed DL buds showed apoplastic connectivity when more developed D buds did not (Fig. 1C; Supplementary Figs S2A, B, S3B). In our view, the local hydrolysis of polysaccharides in the cell wall should contribute to the increase of porosity during early bud burst. Upon inspecting gene expression data from a previous study (grapevine buds grown for 72 h versus 3 h in D and DL condition, Meitha *et al.* 2018), we found that genes coding for both cellulose synthase

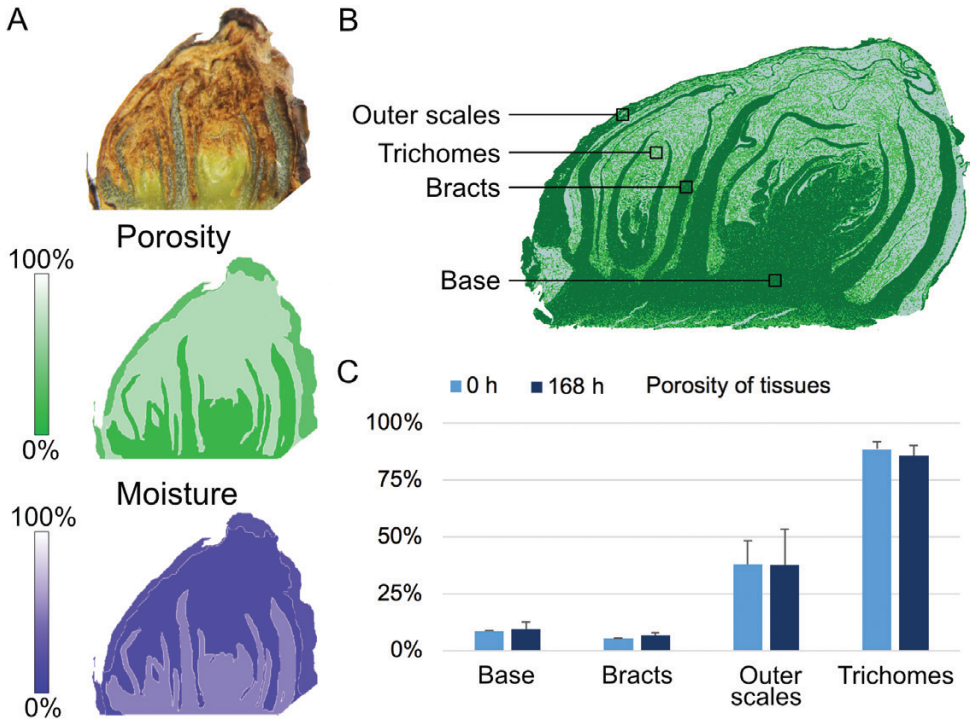

Fig. 5. Porosity and moisture of grapevine buds. (A) At the top, a sectioned bud is shown to depict the three evaluated parts of the bud: the green tissue, the trichomes, and the outer scales. The porosity and the moisture are represented as percentages and were determined by tissue density and weight, respectively. Asterisks indicate statistically significant differences between the different types of tissue using a Tukey comparison (n=5, P<0.0001). (B) Section of a µCT scan representing the four types of tissues evaluated to calculate the porosity by pixel analysis. (C) Comparison of porosity determined by pixel analysis at 0 h and 168 h. Different letters indicate statistically significant differences between the different types of tissue using a Tukey comparison (n=3, P<0.0001). No statistically significant differences were observed between 0 h and 168 h for any type of tissue.

and cellulase were overexpressed at 24 h compared with 3 h but those for cellulase were much more up-regulated than those for cellulose synthase, and the overexpression was greater in the presence of light. For instance, the fold change for genes coding for cellulase was 29 and 43 in D and DL, respectively, whereas the fold change for the genes coding for cellulose synthase was, on average, 2.6 and 5.6 in D and DL, respectively.

Light quality also affects bud burst in rose; in particular, white, blue, and red lights promote bud burst, while far-red light does not, and the bud itself plays an important role in light perception (Girault *et al.*, 2008; Abidi *et al.*, 2013). In grapevine, we recently provided evidence suggesting that cryptochrome photoreceptors play a role in promoting a photomorphogenic response, which points to the importance of blue light (Signorelli *et al.*, 2018). We are not aware of any detailed studies of the light quality responses of grapevine buds.

The meristematic zone of buds is preferentially oxygenated during bud burst

Several studies, particularly in the presence of HC, have identified patterns that implicate the development of oxidative stress and hypoxic response syndromes, which precede the activation of glycolysis, the pentose phosphate pathway, and fermentation, as fundamental events that enable bud burst (Ophir *et al.*, 2009; Vergara *et al.*, 2012). More recently, we observed that even in the absence of HC or other stress, tissue oxygenation and the expression of conserved hypoxia-responsive genes is acute and highly regulated during the first 24 h of bud burst (Meitha *et al.*, 2018). Thereafter, gene expression became more responsive to light and energy cues (Signorelli *et al.*, 2018). Our earlier data also suggested tissue-specific oxygenation of the meristematic core (primary bud complex) after 24 h; however, the resolution of these data was not as clear as previously seen in other organs such as succulent stems (Pedersen *et al.*, 2006). The use of µCT data to map the path of the pO_2 electrode here provides irrefutable evidence that the meristematic core is oxygenated during bud burst. In addition, the O_2 profiles (Fig. 4; Supplementary Fig. S5) provide evidence that the establishment of vascular tissues also promotes oxygenation of the primary bud complex, and that vascular flux may be a significant source of O_2. Moreover, the relatively high porosity of the outer scale determined by the two methodologies here suggests that it is a weak barrier for O_2 and that atmospheric pO_2 (~21 kPa) should be sufficient to oxygenate at least the peripheral regions and tissues of the bud. It would be valuable to extend these studies to the full seasonal dynamics of development and dormancy state of the bud.

Together, our data demonstrate that the pO_2 in the bud is spatially regulated, and that despite the porosity constraints, the meristematic core of the bud (primary meristem) is preferentially oxygenated during bud burst. This oxygenation does not apparently evolve from *in situ* photosynthesis.

Conclusions

We conclude that the apoplastic pore size between the bud and corpus is regulated during bud burst and this regulation

restricts conductance of larger macromolecules until after the sink strength of the bud has established. Light facultatively promotes the rate of this transition. We also conclude that the pO_2 patterns of buds, correlated with the internal structure of the bud, in a way that the lower pO_2 content is observed in the bract structures, whereas the pO_2 of the regions of the trichome hairs and the meristematic core is elevated rapidly once bud burst is initiated. The principles and methods we have demonstrated provide a foundation to explore further the role and regulation of vascular development and tissue oxygen content during the full phenology of the bud.

Supplementary data

Supplementary data are available at *JXB* online.

Table S1. Summary of the assays performed.

Fig. S1. Effect of light on bud burst and bud respiration.

Fig. S2. Apoplastic connectivity in July buds.

Fig. S3. Apoplastic connectivity in August buds.

Fig. S4. Apoplastic connectivity at different incubation times.

Fig. S5. Schematic comparison of eosin Y, acid fuchsin, and rhodamine structures and molecular weights.

Fig. S6. Effect of light on internal O_2 pressure.

Fig. S7. Effect of light on oxygen profiles measurements at 168 h.

Movie S1. Uptake of iodine by grapevine bud at 168 h.

Acknowledgements

We thank Dr Elena L. Coitiño (UdelaR, Uruguay) for her generous help in setting up the computational facilities at the School of Agronomy (UdelaR) and providing the software to perform the computational modelling. The authors acknowledge the facilities and the scientific and technical assistance of the Australian Microscopy & Microanalysis Research Facility at the Centre for Microscopy, Characterisation & Analysis, UWA, a facility funded by the University, State, and Commonwealth Governments. This research was funded by Australian Research Council grants to MJC (LP0990355, DP150103211).

Author contributions

MJC and SS conceived the study; SS carried out biological experiments, and performed all physiological analysis and molecular modelling; JS, ZW, and PV performed and assisted with μCT; DH assisted with respiration measurements; SS analysed the experiments; JAC and MJC advised on experimental design; SS and MJC wrote the manuscript; and all authors approved the manuscript.

References

Abidi F, Girault T, Douillet O, Guillemain G, Sintes G, Laffaire M, Ben Ahmed H, Smiti S, Huché-Thélier L, Leduc N. 2013. Blue light effects on rose photosynthesis and photomorphogenesis. Plant Biology **15**, 67–74.

Alleweldt G, Hofacker W. 1975. Influence of environmental factors on bud burst, flowering, fertility and shoot growth of vines. Vitis **14**, 103–115.

Aloni R, Peterson CA. 1991. Seasonal changes in callose levels and fluorescein translocation in the phloem of *Vitis vinifera* L. IAWA Journal **12**, 223–234.

Aloni R, Peterson CA. 1997. Auxin promotes dormancy callose removal from the phloem of *Magnolia kobus* and callose accumulation and earlywood vessel differentiation in *Quercus robur*. Journal of Plant Research **110**, 37.

Aloni R, Raviv A, Peterson C. 1991. The role of auxin in the removal of dormancy callose and resumption of phloem activity in *Vitis vinifera*. Canadian Journal of Botany **69**, 1825–1832.

Beauvieux R, Wenden B, Dirlewanger E. 2018. Bud dormancy in perennial fruit tree species: a pivotal role for oxidative cues. Frontiers in Plant Science **9**, 657.

Bonhomme M,Peuch M, Ameglio T, *et al*. 2010. Carbohydrate uptake from xylem vessels and its distribution among stem tissues and buds in walnut (*Juglans regia* L.). Tree Physiology **30**, 89–102.

Carpita N, Sabularse D, Montezinos D, Delmer DP. 1979. Determination of the pore size of cell walls of living plant cells. Science **205**, 1144–1147.

Cartechini A, Palliotti A. 1995. Effect of shading on vine morphology and productivity and leaf gas exchange characteristics in grapevines in the field. American Journal of Enology and Viticulture **46**, 227–234.

Considine MJ, Considine JA. 2016. On the language and physiology of dormancy and quiescence in plants. Journal of Experimental Botany **67**, 3189–3203.

Etxeberria E, Gonzalez P, Bhattacharya P, Sharma P, Ke PC. 2016. Determining the size exclusion for nanoparticles in citrus leaves. HortScience **51**, 732–737.

Frisch MJ, Trucks GW, Schlegel HB, *et al*. 2009. Gaussian 09, Revision B.01. Wallingford, UK: Gaussian Inc.

Girault T, Bergougnoux V, Combes D, Viemont JD, Leduc N. 2008. Light controls shoot meristem organogenic activity and leaf primordia growth during bud burst in Rosa sp. Plant, Cell & Environment **31**, 1534–1544.

Heyer AG, Raap M, Schroeer B, Marty B, Willmitzer L. 2004. Cell wall invertase expression at the apical meristem alters floral, architectural, and reproductive traits in *Arabidopsis thaliana*. The Plant Journal **39**, 161–169.

Jmol Team. 2007. Jmol: an open-source Java viewer for chemical structures in 3D. Jmolsourceforgenet.

Jones KS, McKersie BD, Paroschy J. 2000. Prevention of ice propagation by permeability barriers in bud axes of *Vitis vinifera*. Canadian Journal of Botany **78**, 3–9.

Kurepa J, Paunesku T, Vogt S, Arora H, Rabatic BM, Lu J, Wanzer MB, Woloschak GE, Smalle JA. 2010. Uptake and distribution of ultrasmall anatase TiO2 Alizarin red S nanoconjugates in *Arabidopsis thaliana*. Nano Letters **10**, 2296–2302.

Laage D, Elsaesser T, Hynes JT. 2017. Water dynamics in the hydration shells of biomolecules. Chemical Reviews **117**, 10694–10725.

Lavee S, May P. 1997. Dormancy of grapevine buds—facts and speculation. Australian Journal of Grape and Wine Research **3**, 31–46.

Leduc N, Roman H, Barbier F, Péron T, Huché-Thélier L, Lothier J, Demotes-Mainard S, Sakr S. 2014. Light signaling in bud outgrowth and branching in plants. Plants **3**, 223–250.

Maurel K, Leite GB, Bonhomme M, Guilliot A, Rageau R, Pétel G, Sakr S. 2004. Trophic control of bud break in peach (*Prunus persica*) trees: a possible role of hexoses. Tree Physiology **24**, 579–588.

May P, Clingeleffer P, Brien C. 1976. Sultana (*Vitis vinifera* L.) canes and their exposure to light. Vitis **14**, 278–288.

Meitha K, Agudelo-Romero P, Signorelli S, Gibbs DJ, Considine JA, Foyer CH, Considine MJ. 2018. Developmental control of hypoxia during bud burst in grapevine. Plant, Cell & Environment **41**, 1154–1170.

Meitha K, Konnerup D, Colmer TD, Considine JA, Foyer CH, Considine MJ. 2015. Spatio-temporal relief from hypoxia and production of reactive oxygen species during bud burst in grapevine (*Vitis vinifera*). Annals of Botany **116**, 703–711.

Michailidis M, Karagiannis E, Tanou G, Sarrou E, Adamakis ID, Karamanoli K, Martens S, Molassiotis A. 2018. Metabolic mechanisms underpinning vegetative bud dormancy release and shoot development in sweet cherry. Environmental and Experimental Botany **155**, 1–11.

Nicolas WJ, Grison MS, Trépout S, Gaston A, Fouché M, Cordelières FP, Oparka K, Tilsner J, Brocard L, Bayer EM. 2017. Architecture and permeability of post-cytokinesis plasmodesmata lacking cytoplasmic sleeves. Nature Plants **3**, 17082.

Ophir R, Pang X, Halaly T, Venkateswari J, Lavee S, Galbraith D, Or E. 2009. Gene-expression profiling of grape bud response to two alternative dormancy-release stimuli expose possible links between impaired mitochondrial activity, hypoxia, ethylene–ABA interplay and cell enlargement. Plant Molecular Biology **71**, 403–423.

Or E, Vilozny I, Eyal Y, Ogrodovitch A. 2000. The transduction of the signal for grape bud dormancy breaking induced by hydrogen cyanamide may involve the SNF-like protein kinase GDBRPK. Plant Molecular Biology **43**, 483–494.

Or E, Vilozny I, Fennell A, Eyal Y, Ogrodovitch A. 2002. Dormancy in grape buds: isolation and characterization of catalase cDNA and analysis of its expression following chemical induction of bud dormancy release. Plant Science **162**, 121–130.

Parada F, Noriega X, Dantas D, Bressan-Smith R, Pérez FJ. 2016. Differences in respiration between dormant and non-dormant buds suggest the involvement of ABA in the development of endodormancy in grapevines. Journal of Plant Physiology **201**, 71–78.

Pedersen O, Vos H, Colmer TD. 2006. Oxygen dynamics during submergence in the halophytic stem succulent *Halosarcia pergranulata*. Plant, Cell & Environment **29**, 1388–1399.

Petrie PR, Clingeleffer PR. 2005. Effects of temperature and light (before and after budburst) on inflorescence morphology and flower number of Chardonnay grapevines (*Vitis vinifera* L.). Australian Journal of Grape and Wine Research **11**, 59–65.

Possingham JV. 2004. On the growing of grapevines in the tropics. Acta Horticulturae **662**, 39–44.

Rinne PL, Welling A, Vahala J, Ripel L, Ruonala R, Kangasjärvi J, van der Schoot C. 2011. Chilling of dormant buds hyperinduces FLOWERING LOCUS T and recruits GA-inducible 1,3-beta-glucanases to reopen signal conduits and release dormancy in Populus. The Plant Cell **23**, 130–146.

Sánchez LA, Dokoozlian NK. 2005. Bud microclimate and fruitfulness in *Vitis vinifera* L. American Journal of Enology and Viticulture **56**, 319–329.

Signorelli S, Agudelo-Romero P, Meitha K, Foyer CH, Considine MJ. 2018. Roles for light, energy, and oxygen in the fate of quiescent axillary buds. Plant Physiology **176**, 1171–1181.

Skene KG. 1967. Gibberellin-like substances in root exudate of *Vitis vinifera*. Planta **74**, 250–262.

Skene KGM, Antcliff AJ. 1972. A comparative study of cytokinin levels in bleeding sap of *Vitis vinifera* (L.) and the two grapevine rootstocks, salt creek and 1613. Journal of Experimental Botany **23**, 282–293.

Sperry JS, Holbrook NM, Zimmermann MH, Tyree MT. 1987. Spring filling of xylem vessels in wild grapevine. Plant Physiology **83**, 414–417.

Thomson CJ, Armstrong W, Waters I, Greenway H. 1990. Aerenchyma formation and associated oxygen movement in seminal and nodal roots of wheat. Plant, Cell & Environment **13**, 395–403.

Tilsner J, Nicolas W, Rosado A, Bayer EM. 2016. Staying tight: plasmodesmal membrane contact sites and the control of cell-to-cell connectivity in plants. Annual Review of Plant Biology **67**, 337–364.

Vergara R, Rubio S, Pérez FJ. 2012. Hypoxia and hydrogen cyanamide induce bud-break and up-regulate hypoxic responsive genes (HRG) and VvFT in grapevine-buds. Plant Molecular Biology **79**, 171–178.

Xie Z, Forney CF, Bondada B. 2018. Renewal of vascular connections between grapevine buds and canes during bud break. Scientia Horticulturae **233**, 331–338.